Resonant radiation from Peregrine solitons

FABIO BARONIO[1,*], SHIHUA CHEN[2], AND STEFANO TRILLO[3]

[1] INO CNR and Dipartimento di Ingegneria dell'Informazione, Università di Brescia, Via Branze 38, 25123 Brescia, Italy
[2] School of Physics, Southeast University, Nanjing 211189, China
[3] Department of Engineering, University of Ferrara, Via Saragat 1, 44122 Ferrara, Italy
[*] Corresponding author: fabio.baronio@unibs.it

Compiled October 23, 2019

We investigate the phenomenon of resonant radiation emitted by Peregrine solitons. We show that, unlike bright or dark solitons of the nonlinear Schrödinger equation, the radiation process is affected by the intrinsic local longitudinal variation of the soliton wavenumber. We give a phase-matching condition that allows to predict the multiple spectral peaks of the resonant radiation.

http://dx.doi.org/10.1364/XX.XX.XXXXXX

It is well known that fiber solitons supported by the interplay between anomalous group-velocity dispersion and Kerr focusing nonlinearity emit resonant radiation (RR) [1, 2], sometimes termed as Cherenkov radiation [3]. Such RR is constituted by a linear dispersive wave spontaneously growing at a frequency detuning from soliton peak frequency such that phase-matching is achieved owing to the presence of higher-order dispersion. Such radiation plays a key role in supercontinuum generation occurring in gas-filled photonic crystal fibers, being the mechanism that allows for broadening towards the blue-shifted side of the spectrum [4], whereas in other structures such as semiconductor line defect waveguides the RR appears to be red-shifted [5, 6]. The recently renewed interest in such phenomenon has allowed to assess the role of RR in four-wave mixing phenomena [7–9], and, more importantly, the role of wave-breaking and subsequent dispersive shock wave formation as a source of RR when pumping in the normal dispersion regime [10–12], where RR can otherwise be generated by dark solitons (see [13] and references therein). Further investigations have also shown that RR can be enhanced either in microresonator passive cavities by affecting the spectral shape of soliton frequency combs [14–18], or in system exhibiting periodicity [16, 19, 20], which allows for multiple peaks of the emitted RR.

In this letter, we further extend the study of this phenomenon by addressing the radiation emitted by solitons on finite background described by the rational solutions of the focusing nonlinear Schrödinger equation (NLSE). In particular, we focus our attention on the most basic and important of such solutions, namely the fundamental Peregrine soliton (PS) [21], which has been first observed in nonlinear optics [22], although its interest spreads from plasma physics [23] to water waves [24]. Indeed in optics PSs play a key role in phenomena ranging from modulational instability (MI) in fibers [22] to interaction of random waves in integrable turbulence [25] and propagation in quadratic media [26, 27]. The universal nature of PSs stands on the fact that they appear as the local waveshape in the vicinity of the focusing catastrophe point (i.e. wave-breaking occurring in the anomalous dispersion regime for overwhelming nonlinearities), regardless of the shape of the input [28].

Concerning MI, RR was shown to have impact on the spectral shape of spatially recurrent, so-called Fermi-Pasta-Ulam-Tsingou, evolutions [8]. The link of PS to such evolutions arises from the fact that PS is the limit of vanishing modulation frequency of so-called Akhmediev breathers, which separate qualitative different types of recursive behaviors [29]. Nevertheless, the specific mechanism of radiation was not investigated for PS. Here, we show that the emission of radiation from PS can be a highly dynamical process, where, at variance with RR from solitons, the local contribution to the wavenumber arising from the nontrivial phase evolution can bring about new resonance phenomena. Furthermore, our phase-matching argument allows to predict the frequency detuning of the emitted RR accurately, as confirmed by numerical simulations.

We start from the following normalized NLSE, written in the usual notation valid for fiber optics

$$i\psi_z - \frac{\beta_2}{2}\psi_{tt} - i\frac{\beta_3}{6}\psi_{ttt} + |\psi|^2\psi = 0, \tag{1}$$

where $t = (T - Z/V_g)/T_0$, $z = Z/Z_{nl} = Z\gamma P$, T and Z being physical time and distance in lab frame, $T_0 = (|k''|Z_{nl})^{1/2}$ and $Z_{nl} = (\gamma P)^{-1}$ (nonlinear length) are scales associated with power P of the background. Here V_g is the group velocity at carrier frequency ω_0 of the electric field $E(T, Z) = \sqrt{P}\psi(t, z)$, while $\beta_2 = k''/|k''| = -1$ and $\beta_3 = k'''/|k''|T_0$ accounts for second- and third-order dispersion (TOD), respectively. Equation (1) admits, in the limit $\beta_3 = 0$, the rational PS solution over unit background in the form

$$\psi(z, t) = \left[1 - \frac{4(1 + 2iz)}{1 + 4z^2 + 4t^2}\right] \exp(ik_b z) \tag{2}$$

where the exponential term represents the nonlinear Kerr shift of the background. While, due to the adopted normalization, the background nonlinear wavenumber is $k_b = 1$, (corresponding to $k_b Z_{nl}^{-1} = \gamma P$ in real-world units), in the following we stick to the notation k_b to trace its contribution.

As shown in Fig. 1(a) the PS solution (2) represents an initially weak pulse over a finite background which undergoes a

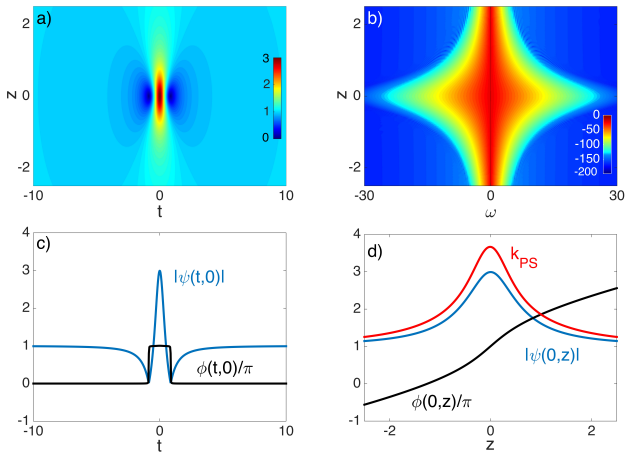

Fig. 1. Unperturbed PS: (a) False color plot of spatio-temporal evolution; (b) Evolution of the Fourier spectrum; (c) amplitude $|\psi(t,z=0)|$ (solid blue) and phase $\phi(t,z=0)/\pi$ (solid black) profile at the point of maximum compression ($z=0$); (d) Longitudinal profiles of amplitude $|\psi(0,z)|$ (solid blue), phase $\phi(0,z)/\pi$ (solid black), and wavenumber k_{PS} from Eq. (4) (solid red), all evaluated at $t=0$.

single cycle of compression and growth followed by broadening and decay. The compression in time domain is accompanied by a strong spectral broadening of the PS, as displayed in Fig. 1(b). Such broadening works as an efficient mechanism of seeding the RR at frequencies that are naturally phase-matched through the contribution of higher-order dispersion. It is well appreciated that, at the maximum compression point $z=0$, the temporal power profile exhibits a peak three times as high as the background and a pair of zeros across which the phase undergoes a jump of π [see Fig. 1(c)], while is less often recognized that the PS exhibits a local (in z) nonlinear deviation of the longitudinal phase, say $\phi_{loc}(t,z)$, from the background phase shift $k_b z$ [24]. Such deviation, which can be regarded as a phase *anomaly* of nonlinear origin (comparing with a continuous wave in the same medium), is intrinsically associated with the localized pulse which lives on top of the background. The overall phase of the PS turns out to be the sum of the background contribution and such local contribution, and reads explicitly as follows

$$\phi_{PS}(t,z) = k_b z + \phi_{loc}(t,z) = k_b z - \tan^{-1}\left(\frac{8z}{4z^2+4t^2-3}\right). \quad \textbf{(3)}$$

The maximum phase anomaly is obtained at the pulse temporal peak $t=0$, and exhibits the longitudinal profile shown in Fig. 1(d). Clearly the z-derivative of such peak phase in Eq. (3) represents the peak nonlinear wavenumber of the PS, which reads

$$k_{PS}(z) = k_b + k_{loc}(z) = k_b + \frac{4(8z^2+6)}{(4z^2+1)(4z^2+9)}, \quad \textbf{(4)}$$

which is made by the constant term k_b of the background, suitably modified by a local contribution (the second term on the RHS). As shown in Fig. 1(d), the wavenumber k_{PS} asymptotically tends to k_b at $z=\pm\infty$, whereas the local contribution becomes strong around $z=0$. In particular, as shown in Fig. 1(d), the longitudinal variation of k_{PS} follows that of the peak intensity, presenting a peak at $z=0$. We anticipate that such local variation can play a relevant role for understanding the features of the RR which are unique to the PSs.

A simple, yet sufficiently accurate, estimate of the radiated frequencies can be obtained by imposing the phase matching condition $k_{RR}(\omega)=k_{PS}$, where k_{RR} is the wavenumber of the linear dispersive waves which constitute the RR at frequency detuning ω from the soliton frequency. Importantly, k_{RR} must be evaluated in the frame where the PS is stationary, that is, in the frame moving with the velocity $v=dt/dz$ of the PS which is induced by the effect of TOD (the unperturbed PS in Eq. (2) has obviously $v=0$). Looking for linear waves in the form $\exp(ik_{RR}z-i\omega\tau)$, where $\tau=t-vz$ is a retarded time, we find from Eq. (1) that the linear part of the wavenumber k_{RR} obeys the dispersion relationship $k_{RR}(\omega)=\frac{\beta_3}{6}\omega^3+\frac{\beta_2}{2}\omega^2-v\omega$. However, one needs to add to this linear expression the nonlinear correction $k_{RR}^{NL}=2k_b$ (equivalent to $2k_b Z_{nl}^{-1}=2\gamma P$ in real-world unit) arising from cross-phase modulation induced by the intense background, on which the linear waves are first generated and then freely propagate [9]. By equating the full (linear and nonlinear) expression k_{RR} to k_{PS} in Eq. (4), we obtain the phase-matching equation

$$\frac{\beta_3}{6}\omega^3+\frac{\beta_2}{2}\omega^2-v\omega=\Delta k_{nl} \quad \textbf{(5)}$$

whose roots $\omega=\omega_{RR}$ yield the RR frequency, corresponding in real-world units to $\Omega_{RR}=\omega_{RR}/T_0=\omega_{RR}(|k''|Z_{nl})^{-1/2}$. In Eq. (5) the term $\Delta k_{nl}=k_{PS}(z)-2k_b=k_{loc}(z)-k_b$ groups all the effective nonlinear contributions. Note that, only in the limit where v and Δk_{nl} become indeed negligible, one obtains the first-order approximation $\omega_{RR}\simeq\tilde{\omega}_{RR}=-3\beta_2/\beta_3$, or the corresponding physical frequency $\Omega_{RR}=3|k''|/k'''$, which has been employed as a rough estimate of the radiation frequency emitted from either solitons or wave-breaking [1, 10, 11]. Except for this limit, Eq. (5) entails that, in general, the phase-matched RR from PSs is affected by the local wavenumber $k_{loc}(z)$, at variance with RR from both bright and dark solitons. Moreover, notice that the nonlinear contribution k_b appears in Eq. (5) with opposite sign compared with bright solitons [3], due to the fact that the RR is emitted over the strong background, similarly to the case of RR from shock waves [9].

The typical phenomenon of RR from a PS in the presence of non-vanishing β_3 is illustrated in Fig. 2, where we report the result of the numerical integration of Eq. (1), with $\beta_3=-0.2$, $\beta_2=-1$. We launch the exact solution (2) taken at $z=-2$ and clearly observe the radiation from the PS in the spatio-temporal evolution shown in Fig. 2(a). One can also notice that TOD induces the radiating PS to drift at a nearly constant velocity $v\neq 0$, contrary to the unperturbed case where $v=0$. A good estimate for such velocity is $v=\beta_3 A^2/6$ where A is the peak amplitude reached by the PS ($A\sim 3$ for a unit background). However, in order to predict more accurately the RR frequency, we estimate the velocity v numerically by a linear fit of the trajectory of the PS peak in the (t,z) plane, around the maximum compression point. The result is shown by the dashed white line in Fig. 2(a) ($v=-0.25$). The radiated linear wave can be clearly seen to depart from the PS, traveling at its own natural velocity $v_{RR}=dk_{RR}/d\omega|_{\omega_{RR}}=\beta_3\omega_{RR}^2/2+\beta_2\omega_{RR}-v$. The evolution of the spectrum shown in Fig. 2(b) clearly shows that the RR lies in the normal dispersion regime and starts to be emitted when the spectrum of the PS is broad enough to efficiently seed the phase-matched frequency ω_{RR}. Such frequency can be estimated as the only real root of the cubic phase-matching Eq. (5). Since its

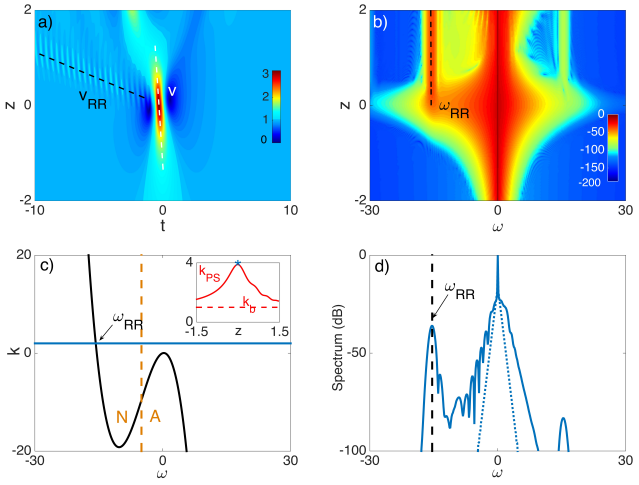

Fig. 2. Propagation of a perturbed radiating PS with $\beta_3 = -0.2$: (a) False color plot of spatio-temporal evolution; dashed white line refers to PS velocity, dashed black line to RR velocity. (b) Corresponding evolution of the Fourier spectrum (log scale); (c) Graphical solution of Eq. (5): ω_{RR} is given by the cross of the blue horizontal line standing for Δk_{NL} evaluated locally at $z = 0$, with the black solid curve signifying the cubic dispersion relation; Inset: PS peak wavenumber k_{PS} evaluated numerically (solid red; blue star is the value at $z = 0$ used to compute Δk_{NL}) and background contribution k_b (dashed red). Dashed vertical orange line refers to zero GVD condition, delimiting the anomalous (A) and normal (N) dispersion regions. (d) Output spectrum in log scale (solid blue) at $z = 2$ compared with input spectrum (dashed blue). Dashed vertical black lines in (b,d) stands for ω_{RR} calculated from (c) at $z = 0$.

closed form expression is cumbersome (root of a cubic polynomial), we resort here to graphically evaluate ω_{RR}, as illustrated in Fig. 2(c), by determining the intersection between the linear dispersive part represented by a cubic polynomial [LHS in Eq. (5)] and the nonlinear contribution [RHS in Eq. (5)] evaluated locally at the onset of the RR ($z = 0$), which corresponds to the horizontal line in Fig. 2(c). The value $\omega_{RR} = -15.8$ determined in this way turns out to be in very good agreement with the RR frequency observed in the numerics, as shown both in Fig. 2(b) and the output spectrum at $z = 2$ reported in Fig. 2(d). Such spectra also clearly show that, once the phase-matched frequency ω_{RR} is sufficiently amplified, also the image frequency $\omega_0 - \Omega_{RR}$ is spontaneously generated via the four-photon mixing process $\omega_0 - \Omega_{RR} = 2\omega_0 - (\omega_0 + \Omega_{RR})$ [30]. Note, however, that such additional frequency remains much weaker (nearly -50 dB) than the phase-matched peak.

For the case shown in Fig. 2, the radiated frequency is well approximated by the first-order expression $\tilde{\omega}_{RR}$, the relative error being only $|\omega_{RR} - \tilde{\omega}_{RR}|/\omega_{RR} \simeq 5\%$. Indeed, in this case, the determination of ω_{RR} turns out to be weakly affected by the value of velocity v as well as by the nonlinear contribution Δk_{NL} (baseline in Fig. 2(c)), due to the locally large slope of the dispersion curve. An important consequence of this is that one has a single real root of Eq. (5), and hence a single radiated frequency, even if one evaluates Δk_{NL} at any different distance z. In other words the baseline Δk_{NL} in Fig. 2(c) crosses the dispersion curve only once, regardless of the z at which k_{NL} is calculated.

When the absolute TOD increases, however, the scenario changes, as illustrated in the example reported in Fig. 3 for $\beta_3 = -0.4$. The spatio-temporal evolution in Fig. 3(a) clearly shows that the RR becomes much stronger, and its emission induces a strong break-up of the PS. In this case the perturbed PS acquires a larger velocity v ($v = -0.7$), which in turn does affect the dispersion curve and hence the value of ω_{RR}. The spectrum in Fig. 3(b) shows a primary RR at lower (compared with previous case) frequency ω_{RR1}, which is emitted again around the maximum compression point $z \sim 0$. Besides the primary peak, one notices in the evolving spectrum the harmonic $2\omega_{RR1}$ of the primary peak as well as the image frequency $-\omega_{RR1}$. The primary frequency ω_{RR1} observed in the simulation is in very good agreement with the graphic solution of Eq. (5) displayed in Fig. 3(c), i.e. the intersection between the dispersion curve and the horizontal blue line corresponding to Δk_{NL} evaluated at $z = 0$.

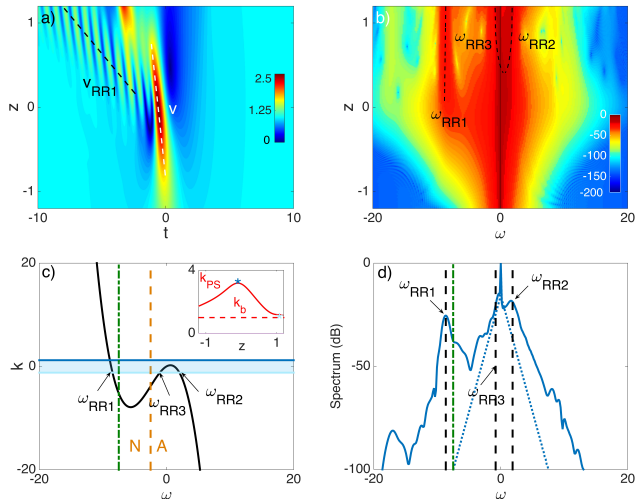

Fig. 3. As in Fig. 2 for $\beta_3 = -0.4$. In (c) the horizontal lines delimiting the pale-blue region, stand for the extremes of $\Delta k_{NL}(z)$: maximum value $\Delta k_{NL}(z = 0)$ (blue line), minimum $\Delta k_{NL}(z = 1.2)$ (cyan line). In the inset the blue and cyan stars on the red solid curve indicate the values of k_{PS} used to compute the blue and cyan horizontal lines, respectively. In (b) the black dashed curves stand for the evolution of ω_{RR1}, ω_{RR2} and ω_{RR3} with z. In (c), (d) the green dashed vertical line stands for the approximation $\tilde{\omega}_{RR}$ to ω_{RR1}. In (d) the black dashed vertical lines stand for ω_{RR1}, ω_{RR2}, ω_{RR3} evaluated at $z = 1.2$.

However, in this case, as the propagation proceeds, the local contribution $k_{loc}(z)$ decreases (see inset in Fig. 3(c)), until the relative $\Delta k_{NL} = k_{loc}(z) - k_b$ is low enough that three real roots appear, corresponding to three different phase-matched frequencies. The latter situation is exemplified by the cyan horizontal line which corresponds to the minimum value $\Delta k_{NL} \simeq -k_b$, obtained at $z = 1.2$. Here, indeed k_{loc} tends to vanish and $k_{PS} \to k_b$ as shown in the inset in Fig. 3(c). The relative horizontal line intersects the dispersion curve in Fig. 3(c) in three points, determining a slight shift of the leftmost intersection corresponding to the primary frequency ω_{RR1}, and, more importantly, two new roots of opposite sign. These correspond to new RR frequencies ω_{RR2} (positive) and ω_{RR3} (negative), which lie close to the pump or PS central frequency ($\omega = 0$), thereby remaining confined in the spectral region of anomalous dispersion, contrary

to ω_{RR1}. At the onset, these two new frequencies are expected to be degenerate ($\omega_{RR2} = \omega_{RR3}$) arising from a doubly degenerate root obtained around $z \simeq 0.4$, where the horizontal line that represents $\Delta k_{NL}(z)$ becomes tangent to the maximum of the cubic dispersion curve in Fig. 3(c). Beyond such distance the two frequencies tend to separate as indicated by the dashed parabolic-like curve reported in the spectral evolution of Fig. 3(b) for $z > 0.4$, which stand for the evolution of $\omega_{RR2}, \omega_{RR3}$ with z, obtained from the graphical solution with a variable $\Delta k_{NL}(z)$. Clearly, in Fig. 3(b), the large spectral content of the PS around $\omega = 0$ hides such frequencies at their onset. However, they start to become visible at larger propagation distances as they becomes sufficiently separated. They are finally clearly visible in the output spectrum at $z = 1.2$ in Fig. 3(d). This spectrum also shows that the primary frequency ω_{RR1} cannot be approximated by $\tilde{\omega}_{RR}$ in this regime of relatively high TOD. The case illustrated in Fig. 3 represents, to the best of our knowledge, the first example of RR with dynamic onset ruled by a local contribution to the wavenumber that in turn reflects the existence of an intrinsic phase anomaly of nonlinear origin.

In order to show how the properties of the RR depend on the effective value β_3 of TOD, we have summarized in Fig. 4 the frequencies of the resonance peaks, namely ω_{RR1}, ω_{RR2} and ω_{RR3}, extracted from numerical simulations corresponding to different values of β_3. As shown the primary branch ω_{RR1} exists for any value of β_3. As the third-order dispersion grows larger, the absolute frequency decreases, or in other words, the radiated peak in the spectrum moves closer to the pump frequency. At the same time the discrepancy with the first-order approximation $\tilde{\omega}_{RR}$ becomes more and more pronounced, thus requiring to evaluate the radiated frequency from the full phase-matching relation in Eq. (5). Conversely, the low frequency components ω_{RR2} and ω_{RR3} start to appear only above a critical absolute value of dispersion $|\beta_{3c}| \simeq 0.25$. Beyond such value, i.e. for $|\beta_3| > |\beta_{3c}|$, the radiated frequency remains nearly unaffected by the value of dispersion. Finally notice that, while we have considered $\beta_3 < 0$, RR emerges also for $\beta_3 > 0$. In this case, the scenarios are identical except for a change of sign of the RR frequencies, which implies that the main peak ω_{RR1} remains located in the normal dispersion region.

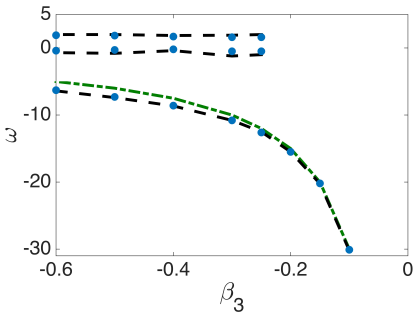

Fig. 4. Global impact of third-order dispersion: frequency ω_{RR1}, ω_{RR2} and ω_{RR3} vs. normalized coefficient β_3. Blue dots: data from numerical simulations; Dashed black curves: theoretical approximation obtained from Eq. (5) with the construction of Fig. 3(c). Green dashed curve: approximation $\tilde{\omega}_{RR} = -3\beta_2/\beta_3$ to ω_{RR1}.

In summary, we have shown that PSs, like bright or dark solitons, or shock waves produced by wave-breaking, radiate linear waves at resonant frequencies in the presence of TOD. However, at variance with the other cases, the radiated frequency can be practically affected, for sufficiently strong TOD, by the local contribution to the wavenumber, which is intrinsic to PS. It is important to emphasize that such local contribution is not unique to the PS, since it is common also to other important solutions, namely Akhmediev and Kuznetsov-Ma breathers, of which PS constitutes a proper limit. We envisage that modifications of the resonant spectra due to the local contribution to the wavenumber could occur as well for those type of breathers, or more generally for recurrent nonlinear evolutions of MI that are sufficiently close to the Akhmediev breather [8, 29].

Funding. National Natural Science Foundation of China (NSFC) (11974075, 11474051).

REFERENCES

1. P. K. A. Wai, C. R. Menyuk, Y. C. Lee, and H. H. Chen, Opt. Lett. **11**, 464 (1986).
2. V. I. Karpman, Phys. Rev. E **47**, 2073 (1993).
3. N. Akhmediev and M. Karlsson, Phys. Rev. A **51**, 2602 (1995).
4. D. V. Skryabin and A. V. Gorbach, Rev. Mod. Phys. **82**, 1287 (2010).
5. N.Y. Joly, J. Nold, W. Chang, P. Hölzer, A. Nazarkin, G. K. L. Wong, F. Biancalana, and P. St. J. Russell, Phys. Rev. Lett. **106**, 203901 (2011).
6. P. Colman, S. Combrié, G. Lehoucq, A. de Rossi, and S. Trillo, Phys. Rev. Lett. **109**, 093901 (2012).
7. M. Erkintalo, Y. Q. Xu, S. G. Murdoch, J. M. Dudley, and G. Genty, Phys. Rev. Lett. **109**, 223904 (2012).
8. J. M. Soto-Crespo, A. Ankiewicz, N. Devine, and N. Akhmediev, J. Opt. Soc: Am. B **29**, 1930 (2012).
9. M. Conforti and S. Trillo, Opt. Lett. **39**, 5760 (2014).
10. K. E. Webb, Y. Q. Xu, M. Erkintalo, and S. G. Murdoch, Opt. Lett. **38**, 151 (2013).
11. M. Conforti and S. Trillo, Opt. Lett. **38**, 3815 (2013).
12. M. Conforti, F. Baronio, and S. Trillo, Phys. Rev. A **89**, 013807 (2014).
13. T. Marest, C. Mas Arabi, M. Conforti, A. Mussot, C. Milian, D.V. Skryabin, and A. Kudlinski, Opt. Lett. **43**, 1511 (2018).
14. S. Wang, H. Guo, X. Bai, and X. Zeng, Opt. Lett. **39**, 2880 (2014).
15. K. Luo, Y. Xu, M. Erkintalo, and S. G. Murdoch, Opt. Lett. **40**, 427 (2015).
16. A. U. Nielsen, B. Garbin, S. Coen, S. G. Murdoch, and M. Erkintalo, APL Photon. **3**, 120804 (2018).
17. V. Brasch, M. Geiselmann, T. Herr, G. Lihachev, M. H. P. Pfeiffer, M. L. Gorodetsky, and T. J. Kippenberg, Science **351**, 357?360 (2016).
18. X. Yi, Q.-F. Yang, X. Zhang, K. Y. Yang, X. Li, and K. Vahala, Nat. Commun. **8**, 14869 (2017).
19. M. Conforti, A. Mussot, A. Kudlinski, and S. Trillo, Sci. Rep. **5**, 9433 (2015).
20. K. Krupa, A.Tonello, A. Barthélémy, and V. Couderc, B. M. Shalaby, A. Bendahmane, G. Millot, and S. Wabnitz, Phys. Rev. Lett. **116**, 183901 (2016).
21. D. H. Peregrine, J. Aust. Math. Soc. Series B, Appl. Math. **25**, 16 (1983).
22. B. Kibler, J. Fatome, C. Finot, G. Millot, F. Dias, G. Genty, N. Akhmediev, and J. M. Dudley, Nat. Phys. **6**, 790 (2010).
23. H. Bailung, S. K. Sharma, and Y. Nakamura, Phys. Rev. Lett. **107**, 255005 (2011).
24. G. Xu, K. Hammani, A. Chabchoub, J. M. Dudley, B. Kibler, and C. Finot, Phys. Rev. E **99**, 012207 (2019).
25. P. Suret, R. El Koussaifi, A. Tikan, C. Evain, S. Randoux, C. Szwaj and S. Bielawski, Nature Commun. **7**, 13136 (2016).
26. F. Baronio, Opt. Lett. **42**, 1756 (2017).
27. F. Baronio, S. Chen, and D. Mihalache Opt. Lett. **42**, 3514 (2017).
28. A. Tikan, C. Billet, G. El, A. Tovbis, M. Bertola, T. Sylvestre, F. Gustave, S. Randoux, G. Genty, P. Suret, and J. M. Dudley, Phys. Rev. Lett. **119**, 033901 (2017).
29. A. Mussot, C. Naveau, M. Conforti, A. Kudlinski, F. Copie, P. Szriftgiser, and S. Trillo, Nat. Photon. **10**, 303 (2018).
30. D. V. Skryabin and A. V. Yulin, Phys. Rev. E **72**, 016619 (2005).

INFORMATIONAL FIFTH PAGE

REFERENCES

1. P. K. A. Wai, C. R. Menyuk, Y. C. Lee, and H. H. Chen, Nonlinear pulse propagation in the neighborhood of the zero-dispersion wavelength of monomode optical fibers, Opt. Lett. **11**, 464 (1986).
2. V. I. Karpman, Radiation by solitons due to higher-order dispersion, Phys. Rev. E **47**, 2073 (1993).
3. N. Akhmediev and M. Karlsson, Cherenkov radiation emitted by solitons in optical fibers, Phys. Rev. A **51**, 2602 (1995).
4. D. V. Skryabin and A. V. Gorbach, Looking at a soliton through the prism of optical supercontinuum, Rev. Mod. Phys. **82**, 1287 (2010).
5. N.Y. Joly, J. Nold, W. Chang, P. Hölzer, A. Nazarkin, G. K. L. Wong, F. Biancalana, and P. St. J. Russell, Bright Spatially Coherent Wavelength-Tunable Deep-UV Laser Source Using an Ar-Filled Photonic Crystal Fiber, Phys. Rev. Lett. **106**, 203901 (2011).
6. P. Colman, S. Combrié, G. Lehoucq, A. de Rossi, and S. Trillo, Blue Self-Frequency Shift of Slow Solitons and Radiation Locking in a Line-Defect Waveguide, Phys. Rev. Lett. **109**, 093901 (2012).
7. M. Erkintalo, Y. Q. Xu, S. G. Murdoch, J. M. Dudley, and G. Genty, Cascaded Phase Matching and Nonlinear Symmetry Breaking in Fiber Frequency Combs, Phys. Rev. Lett. **109**, 223904 (2012).
8. J. M. Soto-Crespo, A. Ankiewicz, N. Devine, and N. Akhmediev, Modulation instability, Cherenkov radiation, and Fermi-Pasta-Ulam recurrence, J. Opt. Soc: Am. B **29**, 1930 (2012).
9. M. Conforti and S. Trillo, Radiative effects driven by shock waves in cavity-less four-wave mixing combs, Opt. Lett. **39**, 5760 (2014).
10. K. E. Webb, Y. Q. Xu, M. Erkintalo, and S. G. Murdoch, Generalized dispersive wave emission in nonlinear fiber optics, Opt. Lett. **38**, 151 (2013).
11. M. Conforti and S. Trillo, Dispersive wave emission from wave breaking, Opt. Lett. **38**, 3815 (2013).
12. M. Conforti, F. Baronio, and S. Trillo, Resonant radiation shed by dispersive shock waves, Phys. Rev. A **89**, 013807 (2014).
13. T. Marest, C. Mas Arabi, M. Conforti, A. Mussot, C. Milian, D.V. Skryabin, and A. Kudlinski, Grayness-dependent emission of dispersive waves from dark solitons in optical fibers Opt. Lett. **43**, 1511 (2018).
14. S. Wang, H. Guo, X. Bai, and X. Zeng, Broadband Kerr frequency combs and intracavity soliton dynamics influenced by high-order cavity dispersion Opt. Lett. **39**, 2880 (2014).
15. K. Luo, Y. Xu, M. Erkintalo, and S. G. Murdoch, Resonant radiation in synchronously pumped passive Kerr cavities Opt. Lett. **40**, 427 (2015).
16. A. U. Nielsen, B. Garbin, S. Coen, S. G. Murdoch, and M. Erkintalo, Emission of intense resonant radiation by dispersion-managed Kerr cavity solitons, APL Photon. **3**, 120804 (2018).
17. V. Brasch, M. Geiselmann, T. Herr, G. Lihachev, M. H. P. Pfeiffer, M. L. Gorodetsky, and T. J. Kippenberg, Photonic chip-based optical frequency comb using soliton Cherenkov radiation,? Science **351**, 357?360 (2016).
18. X. Yi, Q.-F. Yang, X. Zhang, K. Y. Yang, X. Li, and K. Vahala, Single-mode dispersive waves and soliton microcomb dynamics Nat. Commun. **8**, 14869 (2017).
19. M. Conforti, A. Mussot, A. Kudlinski, and S. Trillo, Parametric excitation of multiple resonant radiations from localized wavepackets, Sci. Rep. **5**, 9433 (2015).
20. K. Krupa, A.Tonello, A. Barthélémy, and V. Couderc, B. M. Shalaby, A. Bendahmane, G. Millot, and S. Wabnitz, Observation of Geometric Parametric Instability Induced by the Periodic Spatial Self-Imaging of Multimode Waves Phys. Rev. Lett. **116**, 183901 (2016).
21. D. H. Peregrine, Water waves, nonlinear Schrödinger equations and their solutions J. Aust. Math. Soc. Series B, Appl. Math. **25**, 16 (1983).
22. B. Kibler, J. Fatome, C. Finot, G. Millot, F. Dias, G. Genty, N. Akhmediev, and J. M. Dudley, The Peregrine soliton in nonlinear fibre optics Nat. Phys. **6**, 790 (2010).
23. H. Bailung, S. K. Sharma, and Y. Nakamura, Observation of Peregrine Solitons in a Multicomponent Plasma with Negative Ions Phys. Rev. Lett. **107**, 255005 (2011).
24. G. Xu, K. Hammani, A. Chabchoub, J. M. Dudley, B. Kibler, and C. Finot, Phase evolution of Peregrine-like breathers in optics and hydrodynamics Phys. Rev. E **99**, 012207 (2019).
25. P. Suret, R. El Koussaifi, A. Tikan, C. Evain, S. Randoux, C. Szwaj and S. Bielawski, Single-shot observation of optical rogue waves in integrable turbulence using time microscopy Nature Commun. **7**, 13136 (2016).
26. F. Baronio, Akhmediev breathers and Peregrine solitary waves in a quadratic medium Opt. Lett. **42**, 1756 (2017).
27. F. Baronio, S. Chen, and D. Mihalache, Two-color walking Peregrine solitary waves Opt. Lett. **42**, 3514 (2017).
28. A. Tikan, C. Billet, G. El, A. Tovbis, M. Bertola, T. Sylvestre, F. Gustave, S. Randoux, G. Genty, P. Suret, and J. M. Dudley, Universality of the Peregrine Soliton in the Focusing Dynamics of the Cubic Nonlinear Schrödinger Equation Phys. Rev. Lett. **119**, 033901 (2017).
29. A. Mussot, C. Naveau, M. Conforti, A. Kudlinski, F. Copie, P. Szriftgiser, and S. Trillo, Fibre multiwave-mixing combs reveal the broken symmetry of Fermi-Pasta-Ulam recurrence, Nat. Photon. **10**, 303 (2018).
30. D. V. Skryabin and A. V. Yulin, Theory of generation of new frequencies by mixing of solitons and dispersive waves in optical fibers, Phys. Rev. E **72**, 016619 (2005).